



## Abstract

Very accurate airborne laserscanning (ALS) elevation data was used to calculate the annual volume changes for Hintereisferner and Kesselwandferner in the Ötztal Alps, Austria for 2001/2002–2008/2009. The comparison of the altitude of 51 recently GPS surveyed ground control points showed that the accuracy of the ALS DEMs is better than 0.3 m. The geodetic mass balance was calculated from the volume change using detailed maps of the firn cover and applying corrections for the seasonal snow cover. The maximum snow height at the time of the elevation data flight was 0.5 m averaged over the glacier surface. The volume change data was compared to in situ mass balance data for the total area and at the stakes. For the total period of 8 yr, the difference between the geodetic and the direct mass balance is 2.398 m w.e. on Hintereisferner and 1.380 m w.e. on Kesselwandferner, corresponding to about two times the mean annual mass balance. The vertical ice flow velocity was measured and found to be on the same order of magnitude as the mass balance at KWF. This is an indicator that volume change data does not allow the calculation of ablation or accumulation rates without detailed measurements or models of the vertical ice flow velocity. Therefore, only direct mass balance data allow process studies or investigation of the climatic controls of the resulting mass changes.

## 1 Introduction

The contribution of large glaciers and ice caps to sea level rise, where in situ mass balance data is sparse, is calculated from elevation data produced by various remote sensing methods. Several studies, summarized by Lemke et al. (2007), estimated the quantity of the ice volume change in specific regions. Apart from adding new sensors or regions to the global data base, currently technical questions related to the sensors and the specific accuracies of the elevation products are investigated (Moholdt et al., 2010a,b; Nuth et al., 2010; Nuth and Kääb, 2010; Bollmann et al., 2011). This work is

TCD

5, 565–604, 2011

## Comparison of direct and geodetic mass balances on an annual time scale

A. Fischer et al.

Title Page

Abstract

Introduction

Conclusions

References

Tables

Figures

⏪

⏩

◀

▶

Back

Close

Full Screen / Esc

Printer-friendly Version

Interactive Discussion



very important for estimating the error bars of the current volume change data. But in most cases, the sparse mass balance data allow only very local comparison of volume change to in situ mass balance data. To investigate the consistency of the geodetic and the direct methods of determining glacier mass balance with each other, process oriented studies with accurate field data are necessary.

For small test glaciers with in situ mass balance data in Austria and Norway, very accurate airborne laser scanning (ALS) elevation data was used to calculate the volume change (Geist et al., 2005; Geist and Stötter, 2010). The comparison of the direct to the geodetic net mass balance data showed significant differences (Geist and Stötter, 2010) of up to 100% in 2003, which are clearly not explainable by the error bars of the direct or the geodetic mass balance. Other possible reasons for the discrepancy include different measurement dates, geometric effects, or the density assumption.

The comparison of direct to geodetic mass balance on a multiannual time scale for a number of glaciers indicated that the deviation of the two methods might not be restricted to HEF and KWF, but have a more general nature (Fischer, 2010). Most of the data analyzed within that study is based on photogrammetric DEMs with much lower accuracy than ALS elevation data and is therefore not perfectly suited for a detailed process analysis.

The time series of very accurate ALS elevation data, which is available for Hintereisferner (HEF) and Kesselwandferner (KWF) in the Ötztal Alps, Austria for 2001–2009, provide the perfect database for a process study. The data is complemented by direct mass balance and ice velocity stake data together with a net of ground control points (GCPs) surveyed with differential global positioning system (DGPS) and allow a detailed investigation of the reasons for these differences between the direct and the geodetic method. By analyzing the data of the mass balance years 2001/2002–2008/2009, the following questions are addressed:

## Comparison of direct and geodetic mass balances on an annual time scale

A. Fischer et al.

Title Page

Abstract

Introduction

Conclusions

References

Tables

Figures

⏪

⏩

◀

▶

Back

Close

Full Screen / Esc

Printer-friendly Version

Interactive Discussion



2005 show. KWF (3.9 km<sup>2</sup>) covers about half the area of HEF (7.5 km<sup>2</sup>). Although the maximum elevation of HEF is higher (3750 m a.s.l.) than of KWF (3500 m a.s.l.), the area weighted mean elevation of KWF (3168 m a.s.l.) is higher than that of HEF (3039 m a.s.l.). 64% of the surface area of KWF is located above 3150 m, but only 33% of the area of HEF is as high. The tongue of HEF extends to a lower altitude (2500 m a.s.l.) than KWF (2750 m a.s.l.). 10% of the area of HEF is located below 2750 m a.s.l., and thus below the tongue of KWF. The main aspect of KWF is south east, the tongue of HEF northeast and the firn area from north to east and south. As a result of the different topographies, HEF and KWF show different responses to the same climate forcing (Kuhn et al., 1985), as is evident from the direct mass balance data measured since 1952/1953 (Hoinkes, 1970; Kuhn et al., 1999; Fischer and Markl, 2008). The mean mass balance 1953–2009 was –0.556 m w.e. on Hintereisferner and –0.101 m w.e. on Kesselwandferner. The mean equilibrium line altitude (ELA) 1953–2009 is located at 3135 m a.s.l. on KWF and 2873 m a.s.l. on HEF. From 2002–2009, the mean mass balance was –1.240 m w.e. on Hintereisferner and –0.559 m w.e. on Kesselwandferner and thus significantly more negative as 1953–2009. As a result of these negative mass balance years, between 2001–2009 the glaciers shrunk by 13% (HEF) and 6% (KWF), the firn covered area dropped from 41% to 33% of the total area of HEF and from 61% to 55 % of the total area of KWF (Table 1). In Vent (1908 m a.s.l., Fig. 1), about 6.5 km down the valley from the tongue of KWF and 8 km from the tongue of HEF, a climate station records air temperature and precipitation. The mean annual precipitation at this station for 1952/1953–2008/2009 and 2001/2002–2008/2009 is 661 mm. The highest precipitation rates are in July and August (13% of the annual precipitation each). 72% of the annual precipitation falls between May and November; only 16% from December to February. The mean annual air temperature 1952/1953–2008/2009 is 1.7 °C (2001/2002–2008/2009: 2.3 °C). At 3000 m a.s.l., the precipitation recorded at the rain gauge Hintereisferner is on average twice that recorded in Vent.

**Comparison of direct and geodetic mass balances on an annual time scale**

A. Fischer et al.

Title Page

Abstract

Introduction

Conclusions

References

Tables

Figures

⏪

⏩

◀

▶

Back

Close

Full Screen / Esc

Printer-friendly Version

Interactive Discussion





least 1 point per square meter. The vertical accuracy of airborne laser scanner point measurements is mainly dependent on the point density and the slope angle of the scanned surface (Kraus, 2004). The achieved vertical error is very low for slope angles lower than  $40^\circ$  ( $\pm 0.05$  m) and shows a linear trend. For slopes  $>40^\circ$  an exponential increase of the vertical error can be assumed (1.0 m at  $80^\circ$ ; Bollmann et al., 2011). In comparison with differential GNSS measurements the mean absolute error between GNSS and airborne laser data is about 0.07 m with a very low standard deviation of  $\pm 0.07$  m (Bollmann et al., 2011). This agrees very well with values published by Geist et al. (2005), where they compared differential GNSS measurements with corresponding z-values of a ALS derived DTM of Engabreen (Norway). Their comparison of GNSS z-values with corresponding z-values of the ALS-derived DEMs shows minimal mean deviations of 0.10 m and a standard deviation of  $\pm 0.10$  m, while more than 99.5% of all GNSS point measurements are within a  $\pm 0.30$  m standard deviation. On Hintereisferner and Kesselwandferner, 18 LIDAR DEMS were acquired between 2001 and 2009. Nine of these DEMs were recorded close to the end of the mass balance year and analyzed with this study (Table 2).

### 3.2 Network of ground control points

A net of ground control points (GCPs) was set up during the last century for geodetic surveys close to Hintereisferner and Kesselwandferner. The GCPs are partly located on flat rocks, but are mainly, as is necessary for tachymetric surveys, cylindrically shaped cairns with an iron pole on top. These constructions are 1 to 2 m high and have a diameter of about 0.5 to 0.7 m. Several GCPs are located on buildings. 51 GCPs were revisited between 2007 and 2010 with DGPS to measure the positions in different coordinate systems and to calculate transformation parameters between the various coordinate systems used in the maps of the last 120 yr (Schneider, 1975; Kuhn, 1979; Span, 1997). The results of the surveys are published by Zauner (2010); Niederwald (2009); Weide (2009); Ludwig (2009) and Albrecht (2007). The positions of the GCPs are shown in Fig. 1. The coordinates of the GCPs were determined with

## Comparison of direct and geodetic mass balances on an annual time scale

A. Fischer et al.

Title Page

Abstract

Introduction

Conclusions

References

Tables

Figures



Back

Close

Full Screen / Esc

Printer-friendly Version

Interactive Discussion



three LEICA GPS receivers (system 500) with static long term and short time measurements. The post processing of the data was done with data of the permanent stations of Mals/Malles, Sterzing/Vipiteno (both South Tyrol/Italy), Krahberg, and Patscherkofel (Austria). From all GCP positions, a standard variance of  $6.5 \times 10^{-3}$  m horizontally and  $4.7 \times 10^{-3}$  m vertically with a confidence of 95% was calculated.

### 3.3 Direct mass balance data

The mass balance is measured with the direct glaciological method in the fixed date system as described by Hoinkes (1970), Kuhn et al. (1999), and Fischer and Markl (2008). The mass balance year starts on 1 October and ends on 30 September of the following year. In several field surveys during the mass balance season, not only the ablation, but also the amount of the seasonal snow cover at about 44 stakes on HEF is recorded. Up to 9 snow pits are dug close to 30 September to calculate the mass gain in the higher elevations of HEF. The positions of these stakes and pits are indicated in Fig. 1, the readings closest to the acquisition date of the LIDAR DEM are listed in Table 2. The distribution of the snow cover in the upper part of HEF is monitored with a web cam. On KWF, the main purpose of the 9–10 stakes is the measurement of the ice flow velocity. The stakes are repositioned annually or biannually at the same position. Therefore, the surveys are carried out between 15 August and 15 September. The measured difference in free ends of the stakes is then converted to water equivalent and extrapolated to the mass balance year with the help of the snow pit data and other observations made on HEF.

A possible source of uncertainty in the direct mass balance could be the use of planimetric area and the extrapolation of vertically measured mass balance data from flat to steep areas. As pointed out by Jacobsen and Theakstone (1995), the area of surfaces inclined by an angle of  $\alpha$  is larger than that for flat areas by a factor  $\cos \alpha$ . The relevance of the larger surface area for mass balance was controversially discussed (Rabus et al., 1996; Jacobsen and Theakstone, 1996; Kaser, 1996). Meier (1962) explained why mass balance is defined vertically, and not normal to the glacier surface:

## Comparison of direct and geodetic mass balances on an annual time scale

A. Fischer et al.

Title Page

Abstract

Introduction

Conclusions

References

Tables

Figures

⏪

⏩

◀

▶

Back

Close

Full Screen / Esc

Printer-friendly Version

Interactive Discussion



## Comparison of direct and geodetic mass balances on an annual time scale

A. Fischer et al.

Title Page

Abstract

Introduction

Conclusions

References

Tables

Figures

⏪

⏩

◀

▶

Back

Close

Full Screen / Esc

Printer-friendly Version

Interactive Discussion

this definition is an expedient for the convenience of observers, since it is much easier to measure in the vertical direction than normal to the glacier surface. This clearly refers to glacier areas where the mass balance is measured with stakes or pits. At these flat areas, the difference between the measured vertical mass balance  $b$  and the mass balance normal to the surface  $b_n = b/\cos\alpha$  is small. Assuming that the energy fluxes normal to the surface stay the same for flat and inclined surface areas would result in a vertical mass balance component  $b/\cos\alpha$  in inclined areas. Thus the volume removed by melt from slopes would not be described by multiplying the surface area  $A$  on the map with the vertical mass balance  $b$ , but by multiplying the real surface area  $A/\cos\alpha$  with the component of the mass balance normal to the inclined slope  $b/\cos\alpha$ .

On HEF and KWF, slopes of up to  $83^\circ$  occur. The mean slope is  $15.7^\circ$ . 1% of the glacier area is inclined by more than  $50^\circ$ , 3% by more than  $40^\circ$ , 9% by more than  $30^\circ$ , and 27% by more than  $20^\circ$ . The resulting increase of volume change by accounting for the larger “real” surface area depends on measured mass balance.

### 3.4 Ice flow velocity data

For every point at the glacier surface, elevation changes are the result of ice flow and mass balance. The annual measurements of the  $x$ ,  $y$ , and  $z$  coordinates of the stakes at KWF together with the free ends of the stakes and the surface slope in the vicinity of the stakes allow the calculation of ice thickness changes and the vertical component of ice flow velocity. The ice thickness change at a stake in the field,  $\Delta d$ , and the thickness change caused by accumulation or ablation,  $\Delta a$ , is equal to the vertical component of the ice flow velocity  $v$  when the ice flows a distance of  $y$  (Fig. 2). The vertical component of the ice flow velocity  $v$  is also calculated as difference of the altitude of the stake top  $\Delta z_p$  and the altitude difference in direction of the flow line  $\Delta h$ .

$$v = \Delta d - \Delta a = \Delta z_p - \Delta h \quad (1)$$

On HEF, the ice flow velocity is measured annually at stone line 6 (Fig. 1). The position of the stones placed in this line in mid of August is measured after one year before repositioning the stones. These records allow the calculation of the surface parallel flow path, but not the vertical component of ice flow velocity. The comparison of the flow path of the stones with that of a stake showed that the movement of the stones relative to the surface is smaller than 0.4 m per year. The absolute amount depends on the ablation.

### 3.5 Geodetic mass balance

The specific geodetic mass balance  $b_g$  is calculated by multiplication of the volume difference  $\Delta V$  between two dates  $t_1$  and  $t_2$  with the density of the surface layer  $\rho$  at  $t_1$  divided by the glacier surface area  $A$  at  $t_1$ .

$$b_g = \frac{\Delta V}{A} \cdot \rho \quad (2)$$

The total volume change  $\Delta V$  is derived from the elevation change  $\Delta z = z_{t_2} - z_{t_1}$  at every pixel of the  $1 \times 1$  m LiDAR DEMs acquired at  $t_1$  and  $t_2$ . Therefore, the area of one pixel is  $1 \text{ m}^2$ , and the volume changes is calculated as sum of the elevation changes at every pixel  $i$  of the glacier surface at  $t_1$ :

$$\Delta V = \sum_i \Delta z \quad (3)$$

For every pixel of the glacier surface, the type of the surface area was determined within two classes: glacier ice with a mean density of  $\rho = 917 \text{ kgm}^{-3}$ , and firn with a mean density of  $\rho = 750 \text{ kgm}^{-3}$  (Fig. 3a). Examples of these firn/ice maps are shown for 2001 and 2009 in Fig. 1.

$$b_g = \sum_i \Delta z_i \cdot \rho_i \quad (4)$$

The calculated volume change includes not only changes in glacier mass which are relevant for glacier mass balance, but also the winter snow cover at the time of

## Comparison of direct and geodetic mass balances on an annual time scale

A. Fischer et al.

Title Page

Abstract

Introduction

Conclusions

References

Tables

Figures

◀

▶

◀

▶

Back

Close

Full Screen / Esc

Printer-friendly Version

Interactive Discussion



the acquisition of the DEM. This elevation change resulting from winter snow cover of height  $s$  must be considered for the calculation of the geodetic mass balance. In the accumulation area, snow which fell until 30 September is part of the mass balance, but in the ablation area it leads to an underestimation of the ice melt. An elevation change caused by snow falls after 1 October results in an overestimation of glacier mass also in the accumulation area (Fig. 3b), because the density of the fresh snow is much lower than the usually assumed mean density. When the surface elevation data was recorded before the end of the melt season, the surface at the end of the natural mass balance year is lower than in the DEM. If the melt occurs before 30 September, this results in a differences between the direct mass balance and the geodetic mass balance (Fig. 3c). These errors will balance out if the geodetic mass balance of several years are added.

The volume change was extrapolated from the LiDAR flights to the mass balance year using field observations of snow cover and/or ice melt between the date of the flight and the end of the mass balance year (Fig. 4). The snow cover at the time of the LiDAR flight and the accumulation/ablation between the flight and 30 September was analyzed for every pixel.

## 4 Results

### 4.1 Accuracy of the LiDAR data at the GCPs

The measured altitude of 51 GCPs surrounding HEF and KWF was compared to the elevation of the LiDAR DEMs at the GCPs. The location of these GCPs is indicated in Fig. 1, the GCPs and the results of the comparison area listed in Table 3. Some GCPs are mounted in flat areas, some are cairns (Stm. in Table 3) with tubes (Sta. in Table 3), and very few are located on buildings, such as Brandenburger Haus (BBH), Hochjochospiz (HJH) and Station Hintereis. Since the altitude of the LiDAR DEM at the position of these buildings does not correspond to the altitude of the GCP, and

## Comparison of direct and geodetic mass balances on an annual time scale

A. Fischer et al.

Title Page

Abstract

Introduction

Conclusions

References

Tables

Figures



Back

Close

Full Screen / Esc

Printer-friendly Version

Interactive Discussion





the maximum and the shape of the curve correlate neither with the mass balance nor with the equilibrium line altitude (ELA). In the year 2003, nearly all the area of HEF and KWF is subject to subsidence, and thickness losses of  $-6$  m are quite frequent compared to the other years. In 2003, a rapid increase in flow velocity at the upper parts of glaciers which resulted in a very crevassed glacier surface was observed. This indicates that the shape of the profiles in Fig. 5 is a complex result of ice flow and mass balance, and that, especially in 2003, the subsidence of the total glacier area was a result of a movement of the glacier mass down the valley.

### 4.3 Mass balance of Kesselwandferner

For KWF, The direct mass balance  $b_d$  and the geodetic mass balance  $b_g$  calculated with total glacier area  $A$  and the firn covered area  $A_F$  is summarized in Table 5. Since KWF is surveyed between mid-August and mid-September, in most cases no measured snow cover data for the day of the LiDAR flight is available. Therefore, no correction for the seasonal snow cover  $s$  and the melt between the end of the mass balance year ( $\Delta b$ ) was applied. For 2001–2009, the cumulative geodetic mass balance of  $-5.849$  m w.e. is more negative than the cumulative direct mass balance  $-4.469$  m w.e. The difference of  $1.380$  m w.e. corresponds to the twice annual mean mass balance within the period, or 13% of the total cumulative direct mass balance. The mean annual difference between the geodetic and the direct mass balance is  $0.173$  m w.e. The geodetic mass balance is more negative than the direct in 2002, 2003, 2006, and 2008. The largest differences occur in 2003 and 2006.

### 4.4 Mass balance of Hintereisferner

For HEF, the direct mass balance  $b_d$  and the geodetic mass balance  $b_g$  calculated with total glacier area  $A$  and the firn covered area  $A_F$  is summarized in Table 6. A correction for seasonal snow cover and melt between the LiDAR flight and the end of mass balance year was applied. The mean values of the correction are summarized in

## Comparison of direct and geodetic mass balances on an annual time scale

A. Fischer et al.

Title Page

Abstract

Introduction

Conclusions

References

Tables

Figures

⏪

⏩

◀

▶

Back

Close

Full Screen / Esc

Printer-friendly Version

Interactive Discussion



## Comparison of direct and geodetic mass balances on an annual time scale

A. Fischer et al.

Title Page

Abstract

Introduction

Conclusions

References

Tables

Figures

⏪

⏩

◀

▶

Back

Close

Full Screen / Esc

Printer-friendly Version

Interactive Discussion

Table 6. For 2001–2009, the cumulative geodetic mass balance of  $-12.318$  m w.e. is more negative than the cumulative direct mass balance  $-9.920$  m w.e. As it is the case for KWF, the difference of  $2.398$  m w.e. corresponds to twice the annual mean mass balance within the period, or 13% of the total cumulative direct mass balance. The mean annual difference between the geodetic and the direct mass balance is  $0.300$  m w.e. The geodetic mass balance is more negative than the direct in 2002, 2003, 2004, and 2006. The largest differences occur in 2003 and 2006. Snow cover occurred in 2001, 2005, 2006, and 2007, the height averaged over the glacier surface was  $0.4$  m. Figure 6 shows the snow conditions during or close to the LiDAR flight. Locally, the snow was up to  $1.5$  m high. The melt between the LiDAR flight and the end of the mass balance year affected only a small portion of the glacier area in lower altitudes. Therefore, the elevation change caused by this melt was only a few centimeters averaged over the total glacier surface, although in 2006 after 1 October  $1$  m of ice melted at the tongue of HEF.

A map of the geodetic mass balance and the difference between the geodetic and the direct mass balance are shown for the years 2001/2002 (Fig. 7) and 2002/2003 (Fig. 8). These years represent different shapes of the the volume change curve 5, and the latter shows the largest differences between the two methods. Since the thickness change at every point of the glacier is a result of mass balance and ice flow, the mean annual flow velocity, subsidence, and mass balance measured in the field at line 6 (white bar in Figs. 7 to 8) is given in Table 7. These data suggest that at line 6 the ice flow velocity continuously decreased from  $6.8$  m in 2002 to  $4.9$  m in 2009, with exception of the speed increase in 2003 to  $7.2$  m. The ice thickness change is about  $1$  m less than the mass balance, indicating that the inflow of ice is sufficient to replace a part of the melted ice. Therefore, the measurements indicate that the direct and the geodetic mass balance differ by  $0$ – $1$  m close to line 6. This is confirmed by Figs. 7 and 8.

For 2001/2002, Fig. 7 shows three areas where the mass balances vary widely: in the firn area (1), as a result of submergence, the measured accumulation is much larger. Close to the crevassed tongue of Langtaufererjochferner (2), the direct ablation

is higher than the geodetic, possibly as a result of the inflow of ice. The activity of this tongue is confirmed by ice falls which frequently occurred after the separation from the main glacier in 2000 up to about 2005. In steep areas, the relocation of snow by avalanches results in local mass balance differences (3). At some part of the glacier tongue (4, 5), the direct mass balance is more negative than the geodetic one, which is possibly a result of ice inflow. For 2002/2003, Fig. 8 shows the same general pattern as for 2001/2002. The patchy pattern results from the high number of crevasses that opened in summer 2003 (1). The subsidence at the higher parts of HEF is much higher than the ablation measured there, and from the data it is not clear if this is a result of ice transport or not. Therefore, measurements of flow velocity are needed to investigate the plausibility of the mass balance data by comparing direct to geodetic results.

#### 4.5 Vertical velocity and volume change at the stakes of Kesselwandferner

In contrast to HEF, on KWF the ice flow velocity has been measured at seven stakes for 2001–2009. L2 is the highest stake on KWF indicated in Fig. 1, L10 the lowest one. The field measurements were transformed from Adria height to ellipsoid height by applying the local offset of 52.6978 m determined by Albrecht (2007). The field measurements did not coincide with the LiDAR flights, therefore the measured and LiDAR altitudes differ as a result of mass balance and ice flow (Tables 7, 8 and 9 summarize the measured thickness changes  $\Delta d$ , the thickness change resulting from mass balance  $\Delta a$ , the vertical component of the ice flow velocity  $v$  at the stakes at KWF, and LiDAR ice thickness change  $\Delta z_L$ . In 2003, the high ablation rates led to the loss of several stakes. The sums given in Tables 7 and 9 include all available data, so that the field and LiDAR results given here are not directly comparable. For 2001–2009, the LiDAR DEMs show a subsidence between 2.94 m at L3, where the accumulation is highest, and 37.84 m at the lowest stake. The field measurements of the thickness changes between 2001–2009 differ between 0.25 m (L2) and 0.59 m (L10), indicating a very good correlation of the data for the total period. At the lowest stake L10, only about 6% of the mass loss is replaced by inflowing ice, whereas at L8

### Comparison of direct and geodetic mass balances on an annual time scale

A. Fischer et al.

Title Page

Abstract

Introduction

Conclusions

References

Tables

Figures



Back

Close

Full Screen / Esc

Printer-friendly Version

Interactive Discussion



more than 50% of the ice is replaced. This difference is a result of a reduced inflow to the tongue, which is rapidly developing into a dead ice body Fischer and Markl (2008). The absolute thickness change decreases at L7 with approximately the same rate of ice replacement. At L6, L5, L3, and L2, the ice thickness shrinks, although the mass balance is positive. The calculated vertical component of the ice flow velocity reaches  $-11.16$  m for 2001–2009 at L2, decreasing to  $-1.30$  m at L6. L7 shows an upward motion of  $0.40$  m, L8 of  $3.15$  m. The highest annual upward motion has been measured at L9 in 2009 ( $2.75$  m). In the accumulation area, the downward motion component exceeds the mass balance component by up to 40%. In the ablation area at L8, the vertical upward motion is 60% of the mass balance. As a result, a local difference of a factor of two between ice thickness change and mass balance occurs on KWF.

#### 4.6 The effects of density change, crevasse volume and slope correction shown for HEF 2003

Differences between volume change and the direct mass balance might not only result from density assumptions or different data acquisition times as discussed in the previous sections, but also from a change in the density of the firn layer. The effect of such a density shift is shown by the direct data of HEF in 2003. Due to the unusual weather of this extreme year, a density change is to be expected, and in fact was evident during field surveys. A change of the surface density of the firn area to ice results in a mass balance of  $-3.360$  m w.e. for HEF and  $-2.832$  m w.e. on KWF. The difference of  $0.269$  m w.e. is much smaller on HEF, of which 41% was covered by firn in 2003, compared to a difference of  $1.286$  m w.e. for the 60% firn covered KWF. Changing the mean density of the firn area to  $650 \text{ kg m}^{-3}$ , as is would be the case after a positive mass balance year, results in  $-3.025$  m w.e. for HEF and  $-2.394$  m w.e. for KWF. For the specific year, the result of a variation of the firn density depends on whether the mass in the firn area is lost or gained.

### Comparison of direct and geodetic mass balances on an annual time scale

A. Fischer et al.

Title Page

Abstract

Introduction

Conclusions

References

Tables

Figures

⏪

⏩

◀

▶

Back

Close

Full Screen / Esc

Printer-friendly Version

Interactive Discussion



---

**Comparison of direct  
and geodetic mass  
balances on an  
annual time scale**

---

A. Fischer et al.

Title Page

Abstract

Introduction

Conclusions

References

Tables

Figures

⏪

⏩

◀

▶

Back

Close

Full Screen / Esc

Printer-friendly Version

Interactive Discussion



2003 provides a perfect test year for estimating the effects of crevasse volume in the DEM and for mass balance generally. In 2003, a number of big crevasses were visible. Some might have been covered by snow, but most, especially in the blue ice area, opened during the summer. The representation of crevasses in the DEM depends on the local incidence angle of the LiDAR; also, the depth of the crevasses is underestimated in the LiDAR DEM. As a first guess, all volume changes exceeding  $-7$  m were interpreted as crevasses, resulting in a crevasse volume of  $3 \times 10^6$  m<sup>3</sup> or 7% of the total volume change.

A correction for the larger area of inclined surfaces, i.e. dividing the direct mass balance by  $\cos \alpha$  (Fig. 9), leads to a direct mass balance of  $-1.948$  m w.e. for 2003, still much less than  $b_g$ , since the mass loss at the inclined areas is small. A map of the correction factor  $1/\cos \alpha$  is shown in Fig. 2. This does not account for the extrapolation of mass balance to inclined surfaces, but only for the larger surface area at the slopes.

## 5 Conclusions

The comparison of the LiDAR-derived with DGPS-measured altitudes of the GCPs shows in all years an accuracy better than 0.3 m including the effects of seasonal snow cover. In flat areas, the accuracy can be expected to be even higher. The mean annual mass balance for the investigated period is  $-1.240$  m w.e. on HEF and  $-0.559$  m w.e. on KWF, therefore the period necessary to achieve a relative error lower than 30% under current conditions is at least 2 yr for KWF and 1 yr for HEF. For the the mean mass balance 1953–2009, the period doubles. This rule of a thumb neglects the effects of seasonal snow cover. On HEF and KWF, September and October are among the wettest months, and therefore there is a high likelihood of significant snowfall. The maximum observed mean snow height which occurred during the LiDAR flights 2001–2009 was 0.55 m, corresponding to 100% of the mean annual mass balance on KWF and 50% of the annual mass balance of HEF. Although locally more than 1 m of ice melted between the LiDAR flight and the end of the mass balance year, the affected

area was small. Therefore, the volume change was only a few cm averaged over the glacier area, and therefore negligible. In any case, the two effects compensate for each other when calculating the cumulative geodetic mass balance of a time series, but alter the values for individual years. Although these effects were corrected, and the LiDAR data was extrapolated to the mass balance year, the offset between the geodetic and the direct data remained large with a maximum of 1.277 m w.e. for HEF and 0.989 m w.e. for KWF in 2003. The comparison of the spatial pattern of the direct and geodetic mass balance data correlated with the available flow velocity data on HEF. For KWF, the detailed flow velocity and altitude measurements of the stakes correlate well with the LiDAR data for 2001–2009. The highest vertical ice flow velocity was observed with  $2.75 \text{ m yr}^{-1}$  at stake L9 at KWF. Therefore, the vertical ice flow velocity can be of the same order of magnitude as the mass balance. This suggests that the direct mass balance data in the firn area of HEF is likely to be reliable. At the same time, this is an indicator that volume change data does not allow the calculation of ablation or accumulation, and therefore the interpretation of energy balance, without a detailed measurement or model of the glacier dynamics. Therefore, direct mass balance data is necessary for process studies or the interpretation of climatic controls on volume changes. Accounting for the larger surface area of inclined surfaces leads to correction factors of up to 3 on HEF, but minor changes in the direct mass balance, since the specific mass balance at these steep areas is small. Since stakes in steep slopes are frequently destroyed by avalanches, snow creep and rock fall, it is not clear if the direct mass balance within these areas is basically correct. If the specific mass balance in steep areas has a larger absolute value, the slope correction changes the result of the net balance significantly. The volume of the crevasses which opened in summer 2003 is estimated to account for 7% of the total volume change. The effect of wrong assumptions vary with the glacier area covered by firn and this is larger for KWF than for HEF. 2001–2009, the firn cover shrank by 9% on HEF and by 18% on KWF, resulting in reduced uncertainty of the geodetic mass balance. From the comparison of the volume change to the field data, a contribution of basal melt to the volume change

## Comparison of direct and geodetic mass balances on an annual time scale

A. Fischer et al.

[Title Page](#)[Abstract](#)[Introduction](#)[Conclusions](#)[References](#)[Tables](#)[Figures](#)[Back](#)[Close](#)[Full Screen / Esc](#)[Printer-friendly Version](#)[Interactive Discussion](#)

is possible, but could not be proven with the data analyzed in this study. The evaluation of further DGPS data to find out possible contribution of basal melt is ongoing.

*Acknowledgements.* On the first place, I want to thank all the helping hands in the field. G. Markl measured the mass balance for many decades until 2004, and maintained the stake network. Without the very hard and enthusiastic work of about 50 students, neither the mass balance measurements nor the GPS surveys would have been possible. The field work on Hintereisferner and Kesselwandferner were supported by the Hydrographical survey of the federal government of Tyrol and the Commission of Geophysics of the Austrian Academy of Sciences. The project ALS-X of the Österreichische Forschungsförderungsgesellschaft (FFG) contributed to the funding of the DGPS surveys. The work on this paper was funded by the Herta-Firnberg Grant ZFT 3290 of the Austrian Science Foundation (FWF).

## References

- Albrecht, F.: Präzise GPS Messungen in den Ötztaler Alpen, Master thesis, Hochschule für Angewandte Wissenschaften FH München, Fakultät für Geoinformation, 2007. 571, 579
- Baltsavias, E.: Airborne laser scanning: basic relations an formulas, ISPRS J. Photogramm., 54, 199–214, 1999. 570
- Bollmann, E., Sailer, R., Briese, C., Stötter, J., and Fritzmann, P.: Potential of airborne laser scanning for geomorphologic feature and process detection and quantifications in high alpine mountains, Z. Geomorphol., 54, in press, 2011. 566, 571
- Fischer, A.: Comparison of direct and geodetic mass balances on a multi-annual time scale, The Cryosphere Discuss., 4, 1151–1194, doi:10.5194/tcd-4-1151-2010, 2010. 567
- Fischer, A. and Markl, G.: Mass balance measurements on Hintereisferner, Kesselwandferner, and Jamtalferner 2003 to 2006. Database and results, Zeitschrift für Gletscherkunde und Glazialgeologie, 42, 47–83, 2008. 569, 572, 580
- Geist, T. and Stötter, J.: Airborne laser scanning in glacier studies, in: Remote Sensing of Glaciers. Techniques for topographic, spatial and thematic mapping of glaciers, Taylor and Francis, London, 179–194, 2010. 567, 570
- Geist, T., Elvehø, H., Jackson, M., and Stötter, J.: Investigations on intra-annual elevation changes using multi-temporal airborne laser scanning data: case study Engabreen, Norway, Ann. Glaciol., 42, 195–201, 2005. 567, 571

## Comparison of direct and geodetic mass balances on an annual time scale

A. Fischer et al.

Title Page

Abstract

Introduction

Conclusions

References

Tables

Figures

◀

▶

◀

▶

Back

Close

Full Screen / Esc

Printer-friendly Version

Interactive Discussion



## Comparison of direct and geodetic mass balances on an annual time scale

A. Fischer et al.

Title Page

Abstract

Introduction

Conclusions

References

Tables

Figures

◀

▶

◀

▶

Back

Close

Full Screen / Esc

Printer-friendly Version

Interactive Discussion



- Höfle, B. and Pfeifer, N.: Correction of laser scanning intensity data: data and model-driven approaches, *ISPRS J. Photogramm.*, 62, 415–433, 2007. 570
- Hoinkes, H.: Methoden und Möglichkeiten von Massenhaushaltsstudien auf Gletschern, *Zeitschrift für Gletscherkunde und Glazialgeologie*, 6, 37–90, 1970. 569, 572
- 5 Jacobsen, F. M. and Theakstone, W. H.: The use of planimetric surface area in glacier mass-balance calculations: a potential source of errors, *J. Glaciol.*, 41, 441–444, 1995. 572
- Jacobsen, F. M. and Theakstone, W. H.: A reply to comments on by G. Kaser on “The use of planimetric surface area in glacier mass-balance calculations: a potential source of errors”, *J. Glaciol.*, 42, p. 588, 1996. 572
- 10 Kaser, G.: Comments on “The use of planimetric surface area in glacier mass-balance calculations: a potential source of errors” by Jacobsen and Theakstone, *J. Glaciol.*, 42, p. 589, 1996. 572
- Kraus, K.: Geometrische Informationen aus Photographien und Laserscanneraufnahmen, Walter de Gruyter, Berlin-New York, vol. 1, 516 pp., 2004. 571
- 15 Kuhn, M.: Begleitworte zur Karte des Hintereisferners 1979, 1:10 000, *Zeitschrift für Gletscherkunde und Glazialgeologie*, 16, 117–124, 1979. 571
- Kuhn, M., Markl, G., Kaser, G., Nickus, U., Obleitner, F., and Schneider, H.: Fluctuations of climate and mass balance: different responses of two adjacent glaciers, *Zeitschrift für Gletscherkunde und Glazialgeologie*, 21, 409–416, 1985. 569
- 20 Kuhn, M., Dreiseitl, E., Hofinger, S., Markl, G., Span, N., and Kaser, G.: Measurements and models of the mass balance of Hintereisferner, *Geogr. Ann. A*, 81A, 659–670, 1999. 569, 572
- Lemke, P., Ren, J., Alley, R., Allison, I., Carrasco, J., Flato, G., Fujii, Y., Kaser, G., Mote, P., Thomas, R., and Zhang, T.: Observations: Changes in Snow, Ice and Frozen Ground, in: *Climate Change: The Physical Science Basis. Contribution of Working Group I to the Fourth Assessment Report of the Intergovernmental Panel on Climate Change*, Cambridge University Press, Cambridge, United Kingdom and New York, 2007. 566
- 25 Ludwig, S.: Capturing, Calculation and Presentation of Changes at the Dead Ice of Hintereisferner Using Terrestrial Laser Scanning, Master thesis, Hochschule für Angewandte Wissenschaften FH München, Fakultät für Geoinformation, 2009. 571
- 30 Meier, M.: Proposed definitions for glacier mass budget terms, *J. Glaciol.*, 4, 252–265, 1962. 572
- Moholdt, G., Hagen, J. O., Eiken, T., and Schuler, T. V.: Geometric changes and mass balance

## Comparison of direct and geodetic mass balances on an annual time scale

A. Fischer et al.

Title Page

Abstract

Introduction

Conclusions

References

Tables

Figures

◀

▶

◀

▶

Back

Close

Full Screen / Esc

Printer-friendly Version

Interactive Discussion

of the Austfonna ice cap, Svalbard, *The Cryosphere*, 4, 21–34, doi:10.5194/tc-4-21-2010, 2010a. 566

Moholdt, G., Nuth, C., Hagen, J. O., and Kohler, J.: Recent elevation changes of Svalbard glaciers derived from ICESat laser altimetry, *Remote Sens. Environ.*, 114, 2756–2767, doi:10.1016/j.rse.2010.06.008, 2010b. 566

Niederwald, T.: Festpunktbestimmung mit GPS für Gletscher-Monitoring-Projekte in den Ötztaler Alpen (Tirol), Master thesis, Hochschule für Angewandte Wissenschaften FH München, Fakultät für Geoinformation, 2009. 571

Nuth, C. and Kääb, A.: What's in an elevation difference? Accuracy and corrections of satellite elevation data sets for quantification of glacier changes, *The Cryosphere Discuss.*, 4, 2013–2077, doi:10.5194/tcd-4-2013-2010, 2010. 566

Nuth, C., Moholdt, G., Kohler, J., Hagen, J., and Kääb, A.: Svalbard glacier elevation changes and contribution to sea level rise, *J. Geophys. Res.*, 115, F01008, doi:10.1029/2008JF001223, 2010. 566

Rabus, B., Harrison, W., and Echelmeyer, K.: Comments on “The use of planimetric surface area in glacier mass-balance calculations: a potential source of errors” by Jacobsen and Theakstone, *J. Glaciol.*, 42, p. 588, 1996. 572

Schneider, H.: Die Grundlagen der Vermessungen am Kesselwandferner (Ötztaler Alpen) und die Bewegung des dieses Gletschers in den Haushaltsjahren 1965/66, 1966/67 ud 1967/68, Dissertation, University of Innsbruck, 1970. 597

Schneider, H.: Die Karte des Kesselwandferners 1971 und die Grundlagen der Vermessungen, *Zeitschrift für Gletscherkunde und Glazialgeologie*, XI, 229–244, 1975. 571

Span, N., Kuhn, M., and Schneider, H.: 100 years of ice dynamics of Hintereisferner, Central Alps, Austria, 1894–1994, *Ann. Glaciol.*, 24, 297–302, 1997. 571

Wehr, A. and Lohr, U.: Airborne laser scanning – an introduction and overview, *ISPRS J. Photogramm.*, 54, 68–82, 1999. 570

Weide, S.: Estimating the Height Accuracy of Airborn Laser scanning with GPS and calculation of Glacier Movement at Hintereisferner, Master thesis, Hochschule für Angewandte Wissenschaften FH München, Fakultät für Geoinformation, 2009. 571

Zauner, R.: Glaziologische Analyse der Gletscheroberfläche am Blockgletscher Äusseres Hochebenkar, Hintereisferner und am Kesselwandferner (Ötztaler Alpen), Bachelor thesis, Hochschule für Angewandte Wissenschaften FH München, Fakultät für Geoinformation, 2010. 571



## Comparison of direct and geodetic mass balances on an annual time scale

A. Fischer et al.

**Table 2.** LiDAR DEMs 2001–2009 used to derive the geodetic mass balance on an annual time scale.

LiDAR	closest field surveys HEF	
11 October 2001		8 October 2001
18 September 2002		2 October 2002
26 September 2003		30 September 2003
5 October 2004		30 September 2004
12 October 2005		30 September 2005
8 October 2006	20 September 2006	30 September 2006
11 October 2007		1 October 2007
9 September 2008	9 September 2008	30 September 2008
30 September 2009		27 September 2009

Title Page

Abstract

Introduction

Conclusions

References

Tables

Figures

⏪

⏩

◀

▶

Back

Close

Full Screen / Esc

Printer-friendly Version

Interactive Discussion



**Table 3.** Summary of GPS measured altitudes ( $z_G$ ) of the GCP points, deviation from the average LiDAR elevation 2001–2009  $z_G - \bar{z}_L$  and the deviations from the mean LiDAR elevation for the year  $i$   $\bar{z}_L - z_{L,i}$  in m. Stm...cairn, Sta...tube, KT...triangulation point.

GCP name	$z_G$ m	$z_G - \bar{z}_L$ m	2001	2002	2002	2004	2005	2006	2007	2008	2009
M. Guslar. Stm. Sta	3180.53										
Knöttlen Stm. Sta	3058.35	1.88	-0.06	-0.01	0.01	0.21	-0.27	-0.08	-0.01	0.11	0.09
Ob. Berg 1	2974.73	1.38	0.02	0.18	0.15	0.23	0.15	-0.27	-0.09	-0.55	0.21
V. Hintereis. Stm. S	3491.82	1.87	-0.44	0.09	-0.09	-0.51	0.30	-0.25	-0.09	0.56	0.42
KWsp. Stm. Sta.	3468.40	1.73	0.02	0.22	0.27	0.22	-0.58	-0.06	-0.16	-0.24	0.32
D.sp. Stm. Sta.	3451.97	2.19	-0.37	-0.55	0.40	0.25	-0.24	-0.13	-0.33	-0.55	1.53
Eisner. Stm. Sta. o.	3419.75	1.57	-0.04	0.41	-0.01	0.57	0.00	-0.50	-0.76	-0.23	0.57
Queck. Stm. Sta. o.	3406.52	1.97	0.41	0.33	0.59	0.00	-0.90	-0.25	0.05	-0.57	0.36
Mutspitze. Stm. Sta.	3310.89	1.61	0.13	-0.32	0.11	0.03	-0.30	-0.05	-0.18	0.10	0.49
K. Schrofen Stm. Sta.	3249.71	1.97	-0.38	-0.09	-0.47	0.28	-0.15	-0.15	-0.15	0.12	1.02
H. Guslar n Stm. Sta.	3199.33	2.00	-0.46	0.19	0.24	0.36	-0.28	-0.51	-0.30	0.44	0.33
H. Guslar a w. K.	3200.43	0.37	-0.35	0.17	-0.04	0.19	-0.02	-0.25	-0.04	-0.01	0.38
Schatz Stm. Sta. o.	3001.07	2.01	-1.00	-1.17	0.13	0.33	0.24	0.03	-0.03	-0.05	1.52
Schatz	2999.34	0.09	-0.16	-0.04	0.12	0.14	-0.09	-0.04	0.01	0.02	0.06
Knöttlen Stm. o.	3057.36	0.89	-0.06	-0.01	0.01	0.21	-0.27	-0.08	-0.01	0.11	0.09
Hess	2961.07	2.74	-0.11	-0.40	-0.09	0.31	-0.06	-0.39	0.13	0.27	0.32
Finsterwalder	2858.18	1.94	-0.32	-0.05	0.08	0.18	-0.12	-0.09	-0.15	0.21	0.27
Signal VI	2634.92	0.17	0.16	0.14	0.34	-0.16	-0.17	-0.02	-0.20	-0.12	0.02
Lang	3344.49	-0.08	-0.26	-0.14	0.41	0.02	-0.17	0.05	-0.14	0.15	0.08
BBH SO Giebel	3339.33	4.43	5.50	2.36	-9.37	5.85	-9.09	-0.41	0.27	0.47	
Unter BBH	3319.89	0.33	-0.61	-0.33	-0.35	0.57	0.66	-0.29	0.09	-0.19	0.44
BB Jöchl Stm.	3303.01	2.70	0.24	0.39	0.09	-0.48	-0.59	-1.21	-0.67	2.17	0.05
M. HEisp. Stm.	3504.50	1.87	-0.32	-0.69	-0.18	0.41	0.17	0.25	0.32	-0.31	0.36
Nock Stm. Sta. o.	3206.46	1.76	-0.26	-0.23	0.24	0.44	-0.36	-0.05	-0.07	-0.14	0.42
S. Reutherw. Stm.	3093.07	1.68	0.12	0.33	-0.77	0.64	0.37	-0.17	-0.77	-0.03	0.30
S. Guslarj. Stm.	3420.23	1.49	-0.69	-0.58	0.65	0.31	0.22	0.33	-1.20	0.64	0.34
S. Guslarj. w	3418.13	0.12	-0.03	0.03	0.07	0.06	-0.29	0.01	-0.06	0.07	0.11
HJH Giebel	2475.53		-3.28	-6.36	1.88	0.21	3.15	2.79	0.23	0.39	1.00
25 HP HJH	2476.56	0.41	0.22	-0.27	0.64	-0.10	-0.10	-0.11	-0.18	-0.19	0.11
S. II Stm. F.	2635.73	0.17	0.03	0.05	0.14	0.29	0.02	-0.16	-0.25	-0.15	0.01
S. H. Stm. F.	2493.23										
S. M (Loewe). Stm.	2726.63	2.18	-0.27	-0.13	-0.09	0.15	-0.11	0.10	-0.02	0.30	0.06
Block KWF	2806.83	0.49	-0.47	-0.20	-0.14	-0.07	-0.04	0.24	0.25	0.31	0.13
HP 1 KWF	2804.13	-0.10	-0.26	0.10	0.20	0.17	-0.07	-0.09	-0.01	-0.01	-0.04
HP 2 KWF	2757.33	0.11	-0.30	-0.20	-0.06	-0.03	0.53	-0.12	0.02	-0.08	0.25
HP 3 KWF	2838.53	0.10	-0.10	-0.18	0.08	0.02	0.01	0.05	0.00	0.02	0.10
HP 4 E	2878.83	-0.13	0.08	0.06	0.33	0.04	-0.14	-0.10	-0.06	-0.07	-0.13
HP 5	3416.62	0.14	0.13	-0.06	0.30	-0.13	-0.18	-0.24	-0.12	0.13	0.20
HP 6	3081.53		-0.11	-0.03	0.06	0.05	0.00	0.01	-0.03	0.05	0.02
Schram	2834.96	0.10	0.12	-0.26	0.37	0.11	0.01	-0.22	-0.05	-0.15	0.06
Ambach	2852.50	0.02	0.09	-0.25	0.11	0.08	-0.28	-0.02	-0.04	0.17	0.16
HEF	3049.96	0.06	-0.21	-0.02	0.14	0.06	-0.01	0.02	-0.05	0.00	0.10
Hintereis	3077.58	0.15	-0.17	0.26	0.23	0.00	-0.23	-0.02	-0.13	-0.05	0.10
M. Gus. KT	3180.78										
Fluchtk. KT	3546.19	-0.75	-0.23	0.49	0.90	0.63	-1.00	0.67	-0.29	-1.83	0.66
O. Rofenb. KT	2974.78	-0.01	-0.02	-0.01	0.26	0.02	-0.38	-0.06	0.03	0.13	0.06
Ht. HEF KT	3537.24	0.15	-0.38	0.10	0.14	-0.12	-0.08	-0.02	-0.08	0.24	0.19
KT 11-172	3322.53	0.10	-0.42	0.04	0.16	0.16	-0.12	-0.06	-0.10	0.23	0.12
57-172 HP	3546.19	-0.75	-0.23	0.49	0.90	0.63	-1.00	0.67	-0.29	-1.83	0.66
30 HP	2496.54	0.06	0.05	-0.14	0.12	0.00	0.01	-0.02	-0.03	0.04	-0.02
VP Hoinkes	2794.49	0.23	-0.29	-0.20	-0.35	0.54	0.20	0.06	-0.28	0.12	0.18
AWS Sta.	2494.83	0.08	-0.04	-0.05	0.06	0.10	-0.15	-0.05	0.08	0.03	0.01
mean		0.85	-0.13	-0.07	0.22	-0.04	0.06	-0.20	-0.14	0.00	0.30

**Comparison of direct and geodetic mass balances on an annual time scale**

A. Fischer et al.

Title Page

Abstract Introduction

Conclusions References

Tables Figures

◀ ▶

◀ ▶

Back Close

Full Screen / Esc

Printer-friendly Version

Interactive Discussion



## Comparison of direct and geodetic mass balances on an annual time scale

A. Fischer et al.

Title Page

Abstract

Introduction

Conclusions

References

Tables

Figures

⏪

⏩

◀

▶

Back

Close

Full Screen / Esc

Printer-friendly Version

Interactive Discussion



**Table 4.** Annual average of relative differences of GCP altitudes in the LiDAR DEMs.

year	$\bar{z}_L - z_{L,i}$ in m
2001	-0.16
2002	-0.06
2002	0.14
2004	-0.13
2006	-0.08
2007	-0.14
2008	-0.01
2009	0.28

## Comparison of direct and geodetic mass balances on an annual time scale

A. Fischer et al.

**Table 5.** Direct mass balance  $b_d$  compared to the geodetic mass balance  $b_g$  with total glacier area  $A$  and firn covered area  $A_F$  of KWF.

KWF	$b_d$	$b_g$	$b_d - b_g$		$A_F$	$A$
year	m w.e.	m w.e.	m w.e.	year	km <sup>2</sup>	km <sup>2</sup>
2001/2002	0.017	-0.316	0.333	2001	2.403	3.956
2002/2003	-1.546	-2.535	0.989	2002	2.403	3.946
2003/2004	-0.189	0.106	-0.295	2003	2.268	3.908
2004/2005	-0.059	0.140	-0.199	2004	2.268	3.908
2005/2006	-0.617	-1.327	0.710	2005	2.069	3.904
2006/2007	-0.836	-0.516	-0.320	2006	2.060	3.856
2007/2008	-0.444	-0.702	0.258	2007	2.056	3.821
2008/2009	-0.795	-0.699	-0.096	2008	1.855	3.799
sum	-4.469	-5.849	1.380	2009	1.855	3.735

[Title Page](#)
[Abstract](#)
[Introduction](#)
[Conclusions](#)
[References](#)
[Tables](#)
[Figures](#)
[⏪](#)
[⏩](#)
[◀](#)
[▶](#)
[Back](#)
[Close](#)
[Full Screen / Esc](#)
[Printer-friendly Version](#)
[Interactive Discussion](#)


## Comparison of direct and geodetic mass balances on an annual time scale

A. Fischer et al.

**Table 6.** Direct mass balance  $b_d$  compared to the geodetic mass balance  $b_g$  with total glacier area  $A$  and firn covered area  $A_F$  of HEF.

HEF	$b_d$	$b_g$	$b_d - b_g$		$s$	$\Delta b$	$A_F$	$A$
year	m w.e.	m w.e.	m w.e.	year	m	m	km <sup>2</sup>	km <sup>2</sup>
2001/2002	-0.647	-1.492	0.845	2001	0.55	0.003	3.308	8.045
2002/2003	-1.814	-3.091	1.277	2002	-	0.027	3.308	7.964
2003/2004	-0.667	-0.893	0.226	2003	-	-	2.914	7.838
2004/2005	-1.061	-0.776	-0.285	2004	-	-	2.845	7.555
2005/2006	-1.516	-2.258	0.742	2005	0.30	0.055	2.591	7.474
2006/2007	-1.798	-1.666	-0.132	2006	0.33	-	2.235	7.406
2007/2008	-1.235	-1.015	-0.220	2007	0.43	-	2.110	7.212
2008/2009	-1.182	-1.127	-0.055	2008	-	-	1.645	7.118
sum	-9.920	-12.318	2.398	2009	-	-	1.633	6.989

Title Page

Abstract Introduction

Conclusions References

Tables Figures

◀ ▶

◀ ▶

Back Close

Full Screen / Esc

Printer-friendly Version

Interactive Discussion

## Comparison of direct and geodetic mass balances on an annual time scale

A. Fischer et al.

Title Page

Abstract

Introduction

Conclusions

References

Tables

Figures

⏪

⏩

◀

▶

Back

Close

Full Screen / Esc

Printer-friendly Version

Interactive Discussion

**Table 7.** Ice flow path  $s$ , elevation change  $\Delta z$  and elevation change resulting from mass balance  $\Delta a$  at line 6 on HEF.

year	$s$ m	$\Delta z$ m	$\Delta a$ m
2002	6.8	-3.3	-4.21
2003	7.2	-5.9	-6.60
2004	6.2	-3.4	-3.68
2005	6.3	-4.8	-5.39
2006	6.2	-5.1	-5.21
2007	6.0	-5.8	-5.80
2008	5.2	-4.3	-5.12
2009	4.9	-4.2	-5.10

## Comparison of direct and geodetic mass balances on an annual time scale

A. Fischer et al.

**Table 8.** Difference between in stake elevation between field measurements and LiDAR data. The dates of the field measurements are listed in Tables 9 and 7.

Stake	L2	L3	L5	L6	L7	L8	L10
<i>z</i>	3347.21	3308.35	3231.21	3182.94	3132.68	3090.59	2852.89
year	$\Delta z$ in m						
2001	0.07	−0.70	−1.19	−2.41	−2.18	−3.16	−0.54
2002	−0.31	−0.98	−1.43	−2.80	−2.59	−3.84	−1.17
2003	−0.40	−1.32					
2004	0.08	−0.69	−1.28	−2.83	−2.25	−4.04	−1.68
2005	0.53	−0.40	−0.79	−2.51	−2.13	−3.99	−1.67
2006	−0.08	−0.86	−1.42	−3.13	−2.65	−4.29	−2.18
2007	0.02	−0.86	−1.14	−2.91	−2.54	−3.84	−1.44
2008	−0.08	−0.87	−1.23	−2.99	−2.75	−3.89	−1.25
2009	−0.14	−1.00	−1.58	−3.01	−3.09	−4.47	−2.33
mean	−0.03	−0.85	−1.26	−2.82	−2.52	−3.94	−1.53

Title Page

Abstract

Introduction

Conclusions

References

Tables

Figures

⏪

⏩

◀

▶

Back

Close

Full Screen / Esc

Printer-friendly Version

Interactive Discussion



**Table 9.** Measurements of thickness change  $\Delta d$ , thickness change caused by accumulation or ablation,  $\Delta a$ , vertical component of the ice flow velocity  $v$  at the stakes at KWF compared to the LiDAR ice thickness change  $\Delta z_L$  in m.

L2							
year	$\Delta z_L$	date	date	$\Delta d$	$\Delta a$	$v$	$\Delta z_L - \Delta d$
2002	-0.43	13 Sep 2001	13 Sep 2002	-0.05	1.51	-1.68	-0.38
2003	-2.34	13 Sep 2002	14 Sep 2003	-2.25	-0.63	-1.61	-0.09
2004	0.64	14 Sep 2003	9 Sep 2004	0.25	1.31	-1.14	0.39
2005	0.67	9 Sep 2004	8 Sep 2005	0.18	1.46	-1.24	0.49
2006	-1.08	8 Sep 2005	13 Sep 2006	-0.49	0.73	-1.27	-0.59
2007	-0.12	13 Sep 2006	13 Sep 2007	-0.26	1.48	-1.63	0.14
2008	-0.47	13 Sep 2007	9 Sep 2008	-0.34	0.95	-1.39	-0.13
2009	-0.23	9 Sep 2008	8 Sep 2009	-0.14	1.09	-1.2	-0.09
sum	-3.35			-3.10	7.90	-11.16	-0.25
L3							
2002	0.08	13 Sep 2001	13 Sep 2002	0.37	1.39	-1.14	-0.29
2003	-2.69	13 Sep 2002	14 Sep 2003	-2.34	-1.19	-1.2	-0.35
2004	0.78	14 Sep 2003	9 Sep 2004	0.28	1.01	-0.78	0.50
2005	0.78	9 Sep 2004	8 Sep 2005	0.58	1.72	-1.15	0.20
2006	-1.02	8 Sep 2005	13 Sep 2006	-0.61	0.78	-1.37	-0.41
2007	-0.08	13 Sep 2006	13 Sep 2007	0	1.18	-1.16	-0.08
2008	-0.29	13 Sep 2007	10 Sep 2008	-0.41	0.4	-1.01	0.12
2009	-0.51	10 Sep 2008	8 Sep 2009	-0.41	0.7	-1.1	-0.10
sum	-2.94			-2.54	5.99	-8.91	-0.40
L5							
2002	0.10	13 Sep 2001	12 Sep 2002	0.34	0.7	-0.39	-0.24
2003	-3.09	13 Sep 2002					
2004	0.66		9 Sep 2004				
2005	0.87	9 Sep 2004	8 Sep 2005	0.41	0.72	-0.31	0.46
2006	-1.33	8 Sep 2005	13 Sep 2006	-0.68	-0.43	-0.25	-0.65
2007	-0.20	13 Sep 2006	13 Sep 2007	-0.52	-0.36	-0.12	0.32
2008	-0.31	13 Sep 2007	9 Sep 2008	-0.18	-0.24	-0.04	-0.13
2009	-0.48	9 Sep 2008	8 Sep 2009	-0.21	0.04	-0.19	-0.27
sum	-3.79			-0.84	0.43	-1.30	-0.52
L6							
2002	0.27	13 Sep 2001	12 Sep 2002	0.66	0.53	0.06	-0.39
2003	-3.55	12 Sep 2002					
2004	0.58		9 Sep 2004				
2005	0.70	9 Sep 2004	8 Sep 2005	0.36	0.31	0.01	0.34
2006	-1.17	8 Sep 2005	12 Sep 2006	-0.57	-0.74	0.17	-0.60
2007	-0.05	12 Sep 2006	13 Sep 2007	-0.33	-0.37	-0.04	0.28
2008	-0.35	13 Sep 2007	3 Sep 2008	-0.33	-0.29	0.02	-0.02
2009	-0.85	3 Sep 2008	9 Sep 2009	-0.81	-0.97	0.18	-0.04
sum	-4.42			-1.02	-1.53	0.40	-0.43

**Comparison of direct and geodetic mass balances on an annual time scale**

A. Fischer et al.

Title Page

Abstract Introduction

Conclusions References

Tables Figures

⏪ ⏩

◀ ▶

Back Close

Full Screen / Esc

Printer-friendly Version

Interactive Discussion



**Table 9.** Continued.

L7							
year	$\Delta z$			$d$	$a$	$v$	$dz-d$
2002	-0.29	13 Sep 2001	12 Sep 2002	0.11	-0.45	0.42	-0.40
2003	-2.58	12 Sep 2002	26 Aug 2003	-2.35			
2004	0.33	26 Aug 2003	9 Sep 2004	-0.12	-0.39	0.36	0.45
2005	0.29	9 Sep 2004	8 Sep 2005	0.08	-0.41	0.48	0.21
2006	-1.33	8 Sep 2005	12 Sep 2006	-0.71	-1.2	0.52	-0.62
2007	-0.37	12 Sep 2006	13 Sep 2007	-0.52	-1.03	0.52	0.15
2008	-1.00	13 Sep 2007	2 Sep 2008	-0.65	-0.94	0.42	-0.35
2009	-0.70	2 Sep 2008	25 Aug 2009	-0.54	-0.93	0.43	-0.16
sum	-5.65			-4.70	-5.35	3.15	-0.72

L8							
year	$\Delta z$			$d$	$a$	$v$	$dz-d$
2002	-0.39	28 Aug 2001	30 Aug 2002	0.3	-0.66	0.89	-0.69
2003	-4.16	30 Aug 2002	26 Aug 2003	-3.1	-3.94	0.79	-1.06
2004	2.42	26 Aug 2003	24 Aug 2004	-0.2		1.1	2.62
2005	0.11	24 Aug 2004	25 Aug 2005	0.1	-1.03	1.15	0.01
2006	-1.62	25 Aug 2005	12 Sep 2006	-1.4	-2.59	1.13	-0.22
2007	-0.66	12 Sep 2006	12 Sep 2007	-1.2	-2.37	1.24	0.54
2008	-0.96	12 Sep 2007	2 Sep 2008	-0.8	-1.64	1.03	-0.16
2009	-0.94	2 Sep 2008	25 Aug 2009	-0.4	-1.55	1.22	-0.54
sum	-6.19			-6.70	-13.78	8.55	0.51

L9							
year	$\Delta z$			$d$	$a$	$v$	$dz-d$
2009		2 Sep 2008	25 Aug 2009	-0.99	-3.72	2.75	0.99

L10							
year	$\Delta z$			$d$	$a$	$v$	$dz-d$
2002	-3.34	29 Aug 2001	30 Aug 2002	-2.7	-3.06	0.50	-0.64
2003	-5.55	30 Aug 2002	27 Aug 2003	-5.2	-6.03	0.69	-0.35
2004	-3.32	27 Aug 2003	25 Aug 2004	-3.3	-3.56	0.37	-0.02
2005	-4.03	25 Aug 2004	26 Aug 2005	-4.2	-4.41	0.37	0.17
2006	-5.58	26 Aug 2005	1 Sep 2006	-5.0	-5.28	0.24	-0.58
2007	-5.61	1 Sep 2006	12 Sep 2007	-6.4	-6.51	0.10	0.79
2008	-5.06	12 Sep 2007	2 Sep 2008	-5.1	-5.06	0.07	0.04
2009	-5.35	2 Sep 2008	25 Aug 2009	4.6	-4.31		
sum	-37.84			-27.30	-38.22	2.34	-0.59

**Comparison of direct and geodetic mass balances on an annual time scale**

A. Fischer et al.

Title Page

Abstract Introduction

Conclusions References

Tables Figures

⏪ ⏩

◀ ▶

Back Close

Full Screen / Esc

Printer-friendly Version

Interactive Discussion



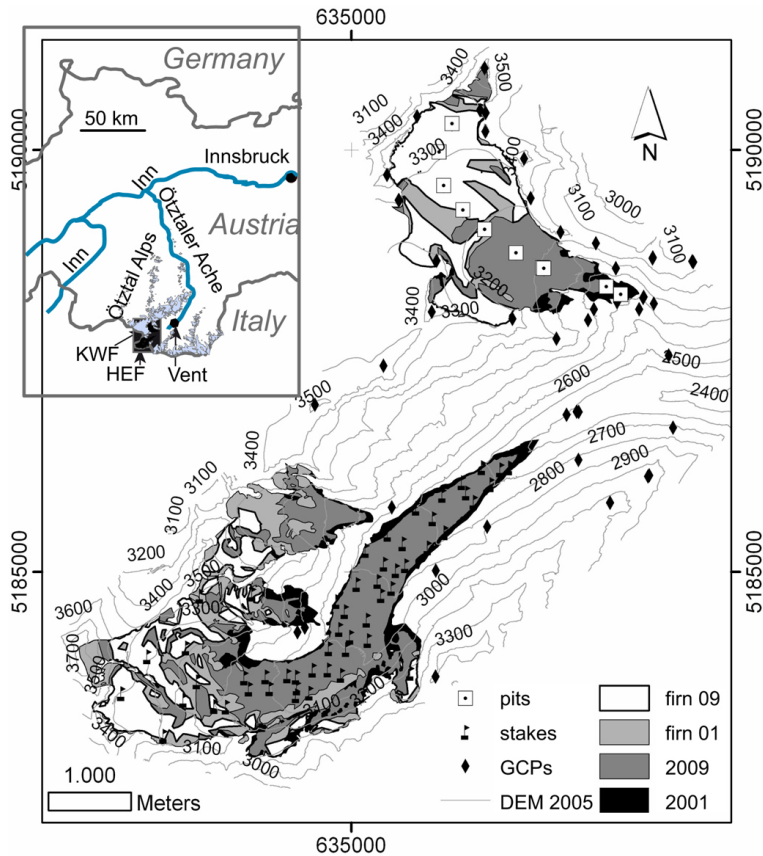


**Fig. 1.** Map of the test sites Hintereisferner (HEF) and Kesselwandferner (KWF). The position of the ground control points (GCPs) and stakes are indicated. The 50 m contour lines show the altitude in October 2005.

**Comparison of direct and geodetic mass balances on an annual time scale**

A. Fischer et al.

[Title Page](#)

[Abstract](#) | [Introduction](#)

[Conclusions](#) | [References](#)

[Tables](#) | [Figures](#)

[◀](#) | [▶](#)

[◀](#) | [▶](#)

[Back](#) | [Close](#)

[Full Screen / Esc](#)

[Printer-friendly Version](#)

[Interactive Discussion](#)



Comparison of direct and geodetic mass balances on an annual time scale

A. Fischer et al.

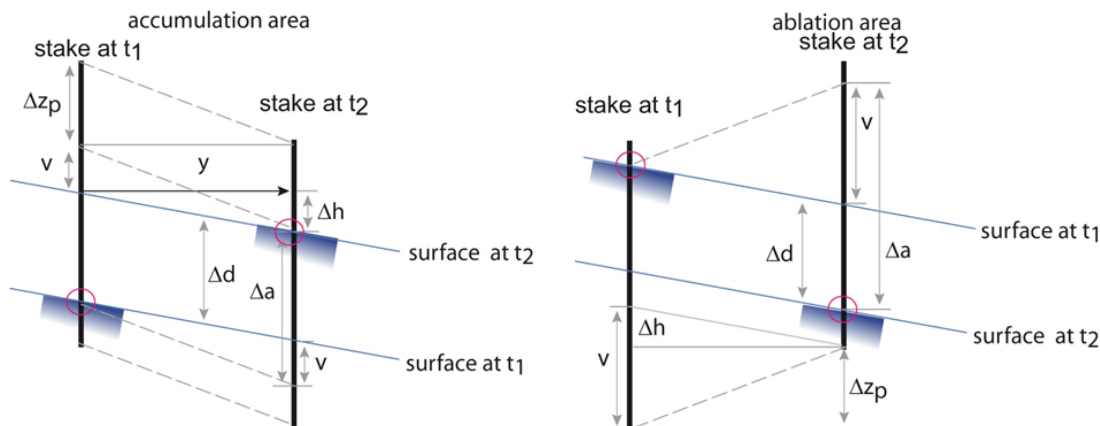


**Fig. 2.** Calculation of the horizontal and vertical ice flow velocity in the accumulation and the ablation area.  $y$  – horizontal travel distance of stake between  $t_1$  and  $t_2$ ,  $t_1$ ,  $t_2$  – dates of measurement,  $v$  – vertical component of the ice flow velocity,  $\Delta a$  – change in free end of the stake as result of mass balance,  $\Delta d$  – change in surface altitude  $d_2 - d_1$ ,  $\Delta h$  – altitude difference in the direction of the flow line, and  $\Delta z_p$  – altitude difference of the stake end (after Schneider, 1970).

Title Page	
Abstract	Introduction
Conclusions	References
Tables	Figures
◀	▶
◀	▶
Back	Close
Full Screen / Esc	
Printer-friendly Version	
Interactive Discussion	

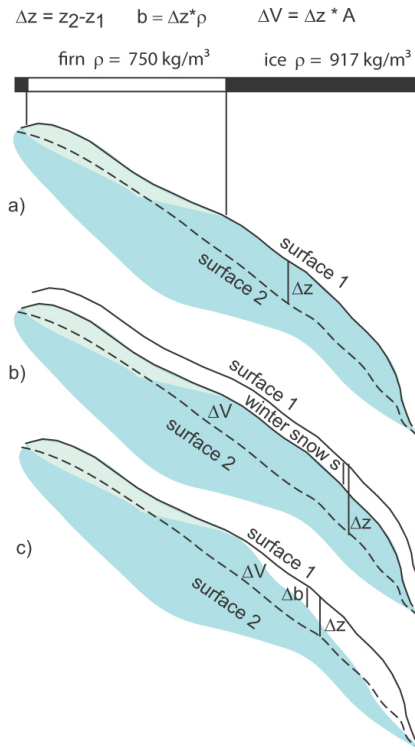


**Fig. 3.** Calculation of the thickness change for every pixel of the DEM from the surface altitude  $z_1$  and  $z_2$  of glacier at time  $t_1$  and  $t_2$ . To calculate the volume change, the thickness change is multiplied with the pixel size and summed up for the glacier area. **(a)** To calculate the specific mass balance  $b$  the density value for every pixel has to be known. **(b)** Fresh snow cover at the time of the LiDAR flight adds additional thickness, but is not relevant for the net mass balance. **(c)** Melt occurring between the end of the mass balance year and the LiDAR flight must be corrected for comparing the geodetic and the direct mass balance.

**Comparison of direct and geodetic mass balances on an annual time scale**

A. Fischer et al.

Title Page	
Abstract	Introduction
Conclusions	References
Tables	Figures
◀	▶
◀	▶
Back	Close
Full Screen / Esc	
Printer-friendly Version	
Interactive Discussion	

## Comparison of direct and geodetic mass balances on an annual time scale

A. Fischer et al.

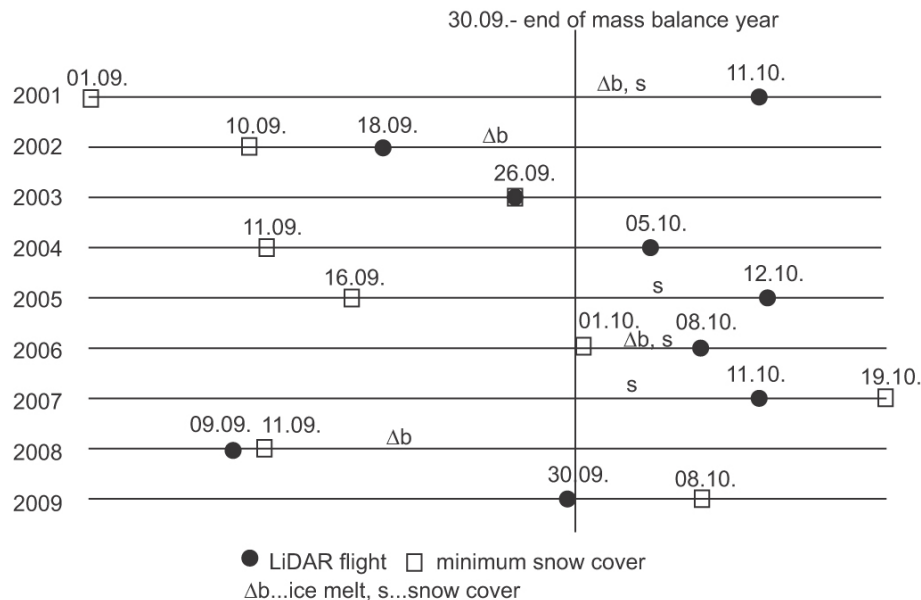


**Fig. 4.** Acquisition dates of the LiDAR DEMs, dates of the minimum snow cover and necessary corrections for snow cover (*s*), and melt between the LiDAR flight and the end of the mass balance year at 30 September ( $\Delta b$ ).

[Title Page](#)
[Abstract](#)
[Introduction](#)
[Conclusions](#)
[References](#)
[Tables](#)
[Figures](#)
[⏪](#)
[⏩](#)
[◀](#)
[▶](#)
[Back](#)
[Close](#)
[Full Screen / Esc](#)
[Printer-friendly Version](#)
[Interactive Discussion](#)

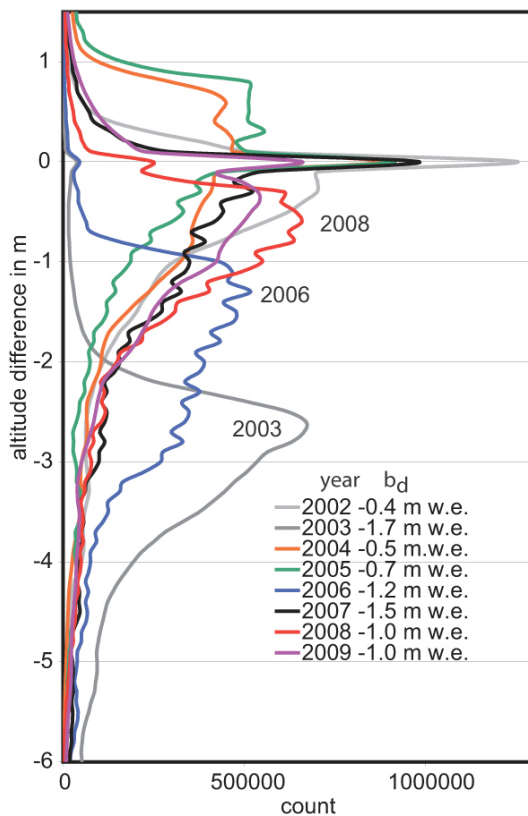


**Fig. 5.** Frequency of altitude changes in m for the mass balance years 2002 to 2009.

**Comparison of direct and geodetic mass balances on an annual time scale**

A. Fischer et al.

Title Page

Abstract Introduction

Conclusions References

Tables Figures

⏪ ⏩

◀ ▶

Back Close

Full Screen / Esc

Printer-friendly Version

Interactive Discussion



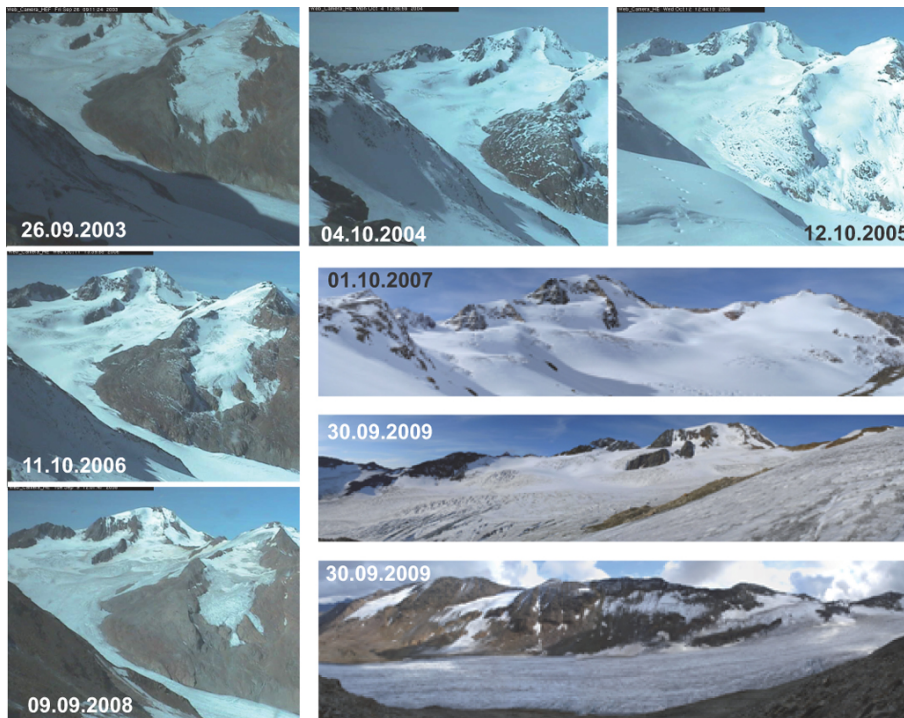


**Fig. 6.** Images of HEF at or close to LiDAR campaigns.

**Comparison of direct and geodetic mass balances on an annual time scale**

A. Fischer et al.

Discussion Paper | Discussion Paper | Discussion Paper | Discussion Paper | Discussion Paper

Title Page

Abstract Introduction

Conclusions References

Tables Figures

⏪ ⏩

◀ ▶

Back Close

Full Screen / Esc

Printer-friendly Version

Interactive Discussion



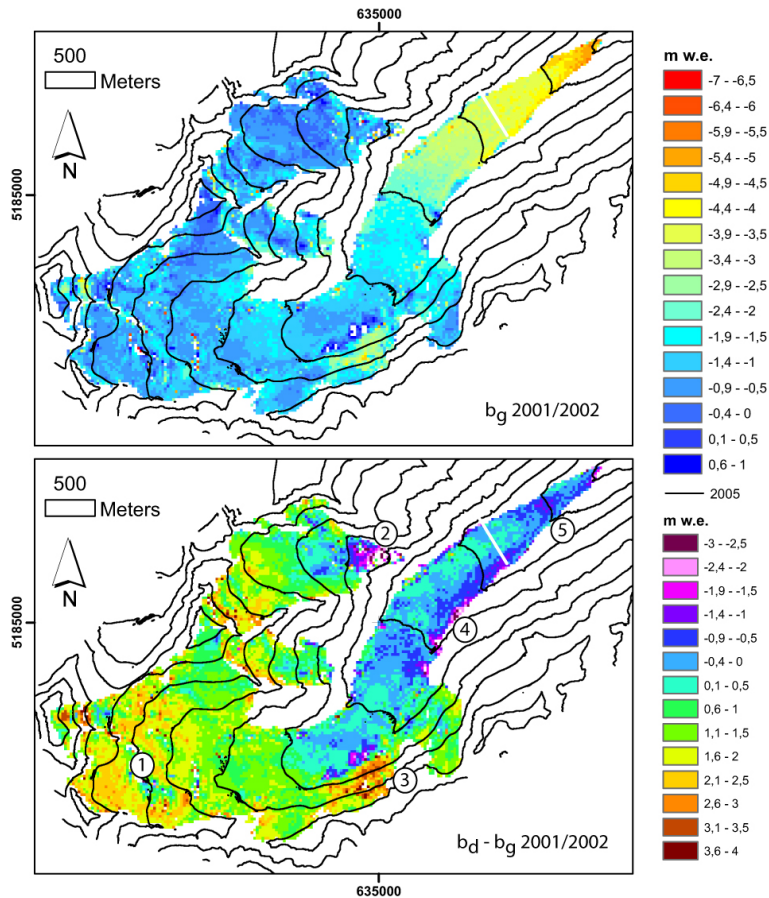


**Fig. 7.** Geodetic mass balance  $b_g$  and difference between the direct and the geodetic mass balance  $b_d - b_g$  for 2001/2002, both in m w.e. The position of the line 6 is indicated with the white bar.

## Comparison of direct and geodetic mass balances on an annual time scale

A. Fischer et al.

Title Page

Abstract

Introduction

Conclusions

References

Tables

Figures



Back

Close

Full Screen / Esc

Printer-friendly Version

Interactive Discussion



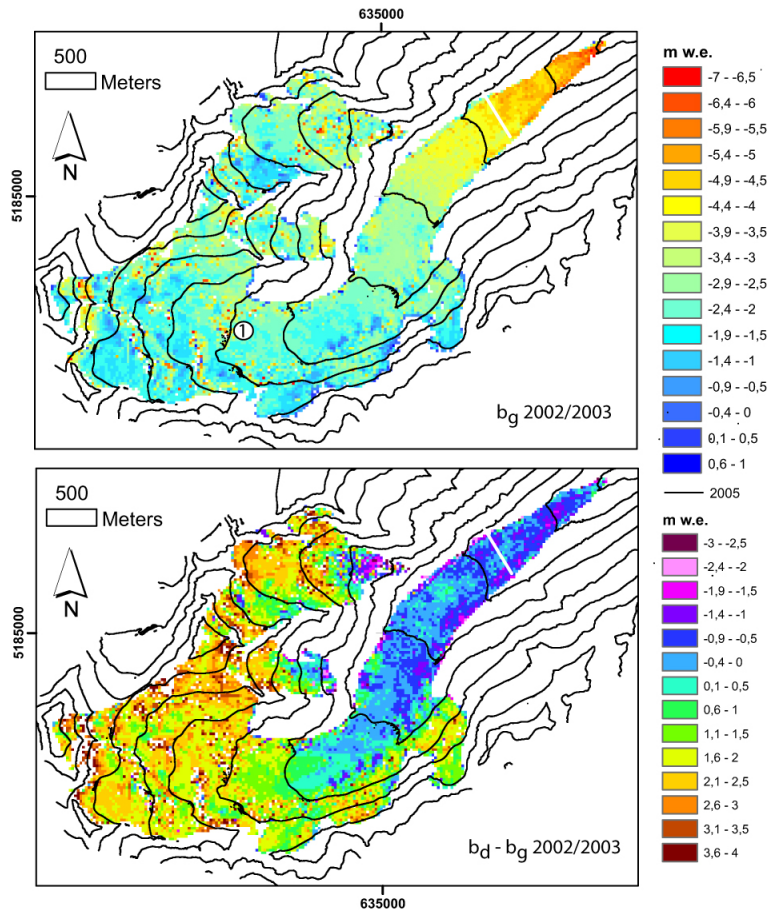


**Fig. 8.** Geodetic mass balance  $b_g$  and difference between the direct and the geodetic mass balance  $b_d - b_g$  for 2002/2003, both in m.w.e. The position of the line 6 is indicated with the white bar.

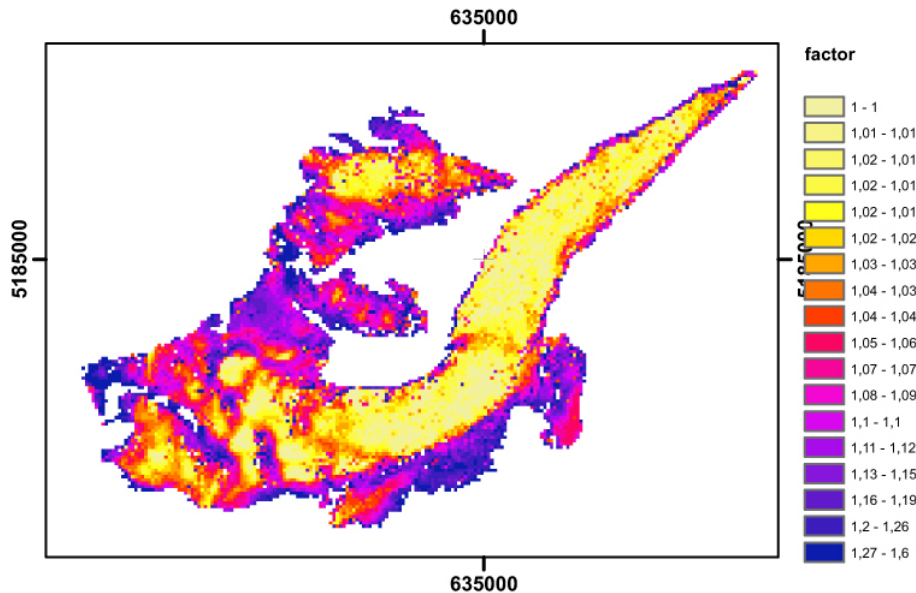


**Fig. 9.** Correction factor  $1/\cos\alpha$  calculated from the LiDAR DEM 2005.

**Comparison of direct and geodetic mass balances on an annual time scale**

A. Fischer et al.

Title Page

Abstract Introduction

Conclusions References

Tables Figures

⏪ ⏩

◀ ▶

Back Close

Full Screen / Esc

Printer-friendly Version

Interactive Discussion

